Biosensors and Bioelectronics 191 (2021) 113405

Contents lists available at ScienceDirect

Biosensors and Bioelectronics

journal homepage: www.elsevier.com/locate/bios

Short communication

# An electroactive and thermo-responsive material for the capture and release of cells

Maite Garcia-Hernando [a,b,1], Janire Saez [c,*,1], Achilleas Savva [c], Lourdes Basabe-Desmonts [b,d,e,f], Róisín M. Owens [c], Fernando Benito-Lopez [a,d,e,**]

[a] Microfluidics Cluster UPV/EHU, Analytical Microsystems & Materials for Lab-on-a-Chip (AMMa-LOAC) Group, Analytical Chemistry Department, University of the Basque Country UPV/EHU, Barrio Sarriena S/n, 48940, Leioa, Spain
[b] Microfluidics Cluster UPV/EHU, BIOMICs Microfluidics Group, Lascaray Research Center, University of the Basque Country UPV/EHU, Avenida Miguel de Unamuno, 3, 01006, Vitoria-Gasteiz, Spain
[c] Department of Chemical Engineering and Biotechnology, Philippa Fawcett Drive, Cambridge, CB3 0AS, UK
[d] Bioaraba Health Research Institute, Microfluidics Cluster UPV/EHU, Vitoria-Gasteiz, Spain
[e] BCMaterials, Basque Centre for Materials, Micro and Nanodevices, UPV/EHU Science Park, 48940, Leioa, Spain
[f] Basque Foundation of Science, IKERBASQUE, María Díaz Haroko Kalea, 3, 48013, Bilbao, Spain

ARTICLE INFO

*Keywords:*
Label-free
Biosensor
Cell capture and release
*T*-responsive
Electrochemical impedance spectroscopy
Smart functional materials

ABSTRACT

Non-invasive collection of target cells is crucial for research in biology and medicine. In this work, we combine a thermo-responsive material, poly(*N*-isopropylacrylamide), with an electroactive material, poly(3,4-ethylenedioxythiopene):poly(styrene sulfonate), to generate a smart and conductive copolymer for the label-free and non-invasive detection of the capture and release of cells on gold electrodes by electrochemical impedance spectroscopy. The copolymer is functionalized with fibronectin to capture tumor cells, and undergoes a conformational change in response to temperature, causing the release of cells. Simultaneously, the copolymer acts as a sensor, monitoring the capture and release of cancer cells by electrochemical impedance spectroscopy. This platform has the potential to play a role in top-notch label-free electrical monitoring of human cells in clinical settings.

Non-invasive collection of flowing cells such as Circulating Tumor Cells (CTCs) (Ruan et al., 2018; Hao et al., 2018; Qian et al., 2015; Gurkan et al., 2011), bacteria (Zhan et al., 2017; Malic et al., 2015), viruses (Xia et al., 2017) or exosomes (Liu et al., 2020; Hisey et al., 2018; Kang et al., 2017) is fundamental for cell biology, diagnosis and prognosis of diseases, cancer research, drug development and regenerative medicine. In these research fields, cells usually need to be analyzed after their collection, so guaranteeing their viability during the process is essential. The most popular and conventional approaches for the collection of target cells include density-gradient centrifugation (Lu et al., 2015; Johnson et al., 2012), flow cytometry (Bhagwat et al., 2018; Gaysinskaya et al., 2014) and immunomagnetism (Legut and Sanjana, 2019), which are complex and laborious, and require size-dependent sorting (Yamada et al., 2017; Henry et al., 2016).

Immunocapture based biosensors bring selectivity for the target cells (Rabie et al., 2019; Fathi et al., 2018), using specific cell-ligand interactions, which are valuable for specific capture, taking advantage of biochemically modified particles. Specific aptamer (Cao et al., 2017; Li et al., 2016; Shen et al., 2013) and DNA (Bombera et al., 2012; Zhao et al., 2012) ligands are useful for the capture and release of cells, due to specific cell binding nucleic acid sequences. In these cases, cell release is enzymatically triggered, cutting the ligand at a restriction point. However, a system with no enzymatic release would ensure the non-invasiveness for the cells during their capture and release, by using specific ligand-cell bonding based systems.

The popularity of hybrid functional materials is rising for non-invasive cell capture and release. Poly(*N*-isopropylacrylamide) (pNIPAAm) is a thermo-responsive polymer with a lower critical solution

* Corresponding author. Philippa Fawcett Drive, Cambridge, CB3 0AS, UK.
** Corresponding author. Facultad de Farmacia, Paseo de la Universidad, 7, 01006, Vitoria-Gasteiz, Spain.
*E-mail addresses:* maite.garciah@ehu.eus (M. Garcia-Hernando), js2409@cam.ac.uk, js2409@cam.ac.uk (J. Saez), as3024@cam.ac.uk (A. Savva), lourdes.basabe@ehu.eus (L. Basabe-Desmonts), rmo37@cam.ac.uk (R.M. Owens), fernando.benito@ehu.eus, fernando.benito@ehu.eus (F. Benito-Lopez).
[1] Both authors contributed equally.

https://doi.org/10.1016/j.bios.2021.113405
Received 20 March 2021; Received in revised form 13 May 2021; Accepted 1 June 2021
Available online 5 June 2021
0956-5663/© 2021 The Authors. Published by Elsevier B.V. This is an open access article under the CC BY-NC-ND license (http://creativecommons.org/licenses/by-nc-nd/4.0/).

temperature (LCST) phase transition in water at 32 °C (Umapathi et al., 2015). Below the LCST, the polymer is hydrophilic, swelling due to hydrogen bond interactions between chains. When the temperature is above the LCST, conformational changes cause the disruption of the hydrogen bonding interactions, causing the material to shrink (Gallagher et al., 2014). Due to the LCST compatibility with cellular viability, pNIPAAm is useful to modulate cellular adhesion/detachment (Choi et al., 2019).

The use of functionalized pNIPAAm networks for the capture and release of cells, triggered by a change in temperature, has been reported before (Wang et al., 2016; Liu et al., 2013a,b; Hou et al., 2013; Gurkan et al., 2011). The working principle consisted in the capture of CTCs at 37 °C, on pNIPAAm functionalized with cell adhesion moieties. The release was triggered by cooling the material below 32 °C, changing the conformation and topography of pNIPAAm. pNIPAAm is a versatile polymer whose combination with other materials can generate new hybrid functional materials with improved physicochemical properties. As an example, Hao et al. combined temperature-responsive pNIPAAm with light-responsive spiropyran molecules to generate polymeric brushes capable of capture and release cells (Hao et al., 2018). Although these systems allow non-invasive and specific capture and release of target cells, fluorescent labels are required for the monitoring of the collected cells due to the presence of external labels.

Bioelectronics devices enable non-invasive monitoring of cellular processes, providing label-free and non-invasive information on cell processes such as growth and differentiation (Chawla et al., 2018; Reitinger et al., 2012). Bioelectronics have already been used to monitor cell capture and release (Cao et al., 2017; Gao et al., 2016). For instance, Gao et al. (2016) designed a capture and release system based on ferrocene (Fc) and β-cyclodextrin (β-CD). By applying a reduction voltage, the uncharged Fc can bind to the β-CD, which is immobilized on the electrode surface. Cells are released as a result of the electrochemical oxidation. Later, Cao et al. (2017) presented a nanochannel-ion channel, functionalized with an aptamer, for the capture and enzymatic release of cells continuously measuring the ion flow through the nanochannel. They reported a decrease of the ion flow due to cell adhesion, which was recovered after the release. Therefore, the combination of electroactive materials with pNIPAAm could allow the non-invasive monitoring of cell capture and release, providing real-time information without disturbing cellular wellbeing.

Electrochemical impedance spectroscopy (EIS) is a technique that applies an alternating current (AC) across a system, and measures the output current over a frequency range. Due to the low voltages required, and the AC operation, EIS is compatible with biological systems, providing mid-throughput and label-free biosensing at the electrode/biology/electrolyte interface (Rivnay et al., 2015; Jimison et al., 2012; Steinem et al., 1997). EIS has been applied for the automatic, sensitive and quantitative monitoring of many cellular processes (Stolwijk and Wegener, 2019; Curto et al., 2018; Kumar et al., 2015; Ke et al., 2011; Bird and Kirstein, 2009). Poly(3,4-ethylenedioxythiopene):poly(styrene sulfonate) (PEDOT:PSS) is a widely used conducting polymer in the bioelectronics field, due to its mixed ionic and electronic conduction properties, stable operation in aqueous electrolytes, and easy processing (Fan and Ouyang, 2019, Xia, Yijie and Ouyang, 2012). Conducting polymer based electrodes have previously been used for monitoring cell attachment and proliferation by EIS, measuring the change in impedance caused by cell adhesion on PEDOT:PSS (Iandolo et al., 2020; Del Agua et al., 2018).

In this work, we report an electroactive functional copolymer (PEDOT:PSS/pNIPAAm) created by the combination of PEDOT:PSS and pNIPAAm, which combines the conducting properties of the first and the thermo-actuation capabilities of the second. This material enables the label-free capture and release of cells with simultaneous EIS monitoring of the process (Fig. 1A).

To validate the capture and release performance of the system, we used the well-known SW480 cell line from a primary colon adenocarcinoma (Hartman et al., 2009; Wang et al., 2004; Leibovitz et al., 1976). SW480s are considered responsible for tumor initiation, development and metastasis, and have been previously used as model samples to evaluate capture and release systems (Cui et al., 2020; Song et al., 2019).

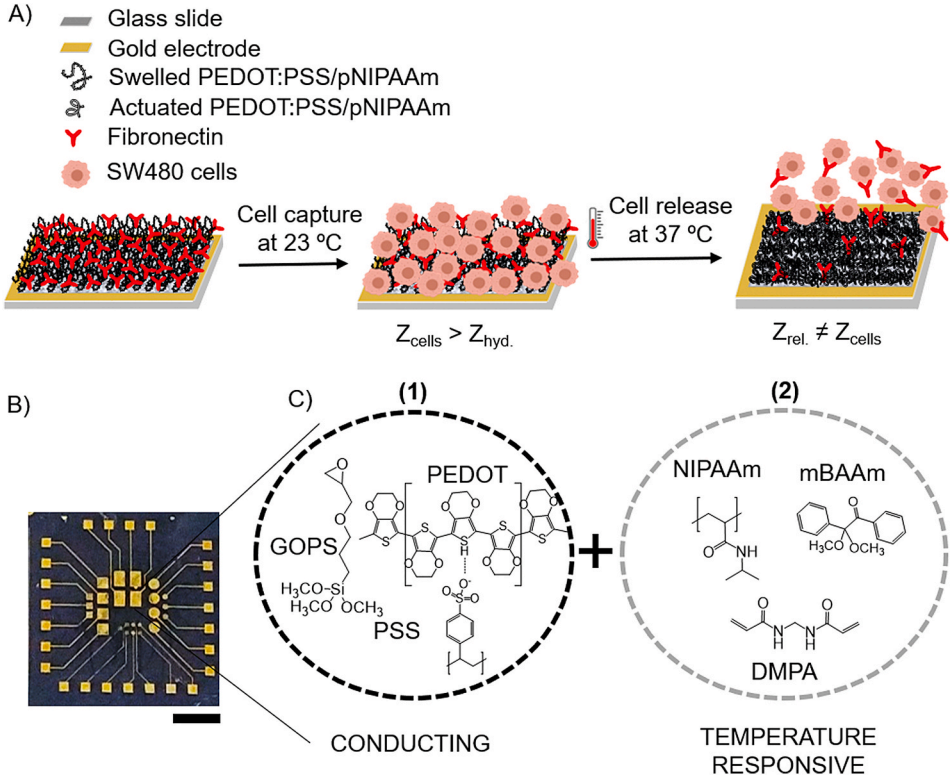


**Fig. 1.** A) Schematics of the mechanism of cell capture and release and electrical monitoring processes based on the hybrid functional PEDOT:PSS/pNIPAAm copolymer. B) Photograph showing the photolithographically patterned device consisting of a 24 gold-electrode array on glass. Scale bar corresponds to 5 mm. C) Chemical structure of the components of (1) the conducting polymer: PEDOT and PSS with GOPS temperature induced crosslinker and (2) the thermo-responsive polymer comprised of NIPAAm as the monomer, mBAAm as the crosslinker and DMPA as photoinitiator. (For interpretation of the references to colour in this figure legend, the reader is referred to the Web version of this article.)

Fibronectin (FN) was embedded into the PEDOT:PSS/pNIPAAm, to induce cell adhesion at room temperature, cutting down incubation times to 3 h. An increase of the temperature to 37 °C induces the copolymer to shrink and subsequent cell release. FN is a widely used extracellular matrix protein that has demonstrated to adhere to the integrins of the cellular membrane, which are crucial in the metastasis led by SW480 cells (Cantor et al., 2015; Bartolome et al., 2014), since they contribute to chemo-resistance of cells to certain anticancer drugs (Liu et al., 2013a,b) and promote epithelial-to mesenchymal transition (Shen et al., 2016; Gupta et al., 2013).

We engineered PEDOT:PSS/pNIPAAm covered gold-electrodes fabricated by photolithography (Fig. 1B and section 1 in the SI, SI-Fig. 1), which enable cell capture and temperature induced release, combined with *in situ* electrical monitoring. This combination led to a copolymer capable of acting simultaneously as an actuator for triggered cell release, and as a sensor, monitoring the process by electrochemical impedance. A copolymer layer was synthesized over the electrodes (section 2 in the SI), by blending two polymer precursors; one photoactive, consisting of *N*-isopropylacrylamide (NIPAAm), the crosslinker *N,N′*-methylene- bis(acrylamide) (mBAAm) and the photoinitiator 2,2-dimethoxy-2-phenylacetophenone (DMPA); and a second PEDOT:PSS with a temperature polymerization initiator, (3-glycidoxypropyl)trimethoxysilane (GOPS) (Fig. 1C). After spin-casting on the electrodes, they were soft-baked at 70 °C, to trigger the polymerization of PEDOT:PSS via GOPS activation. The samples were then exposed to UV light for 1 min to polymerize the pNIPAAm/mBAAm by radical chain-growth polymerization initiated by DMPA after UV activation, followed by a hard-bake at 120 °C to fully crosslink the copolymer. SEM images of the PEDOT:PSS polymer and PEDOT:PSS/pNIPAAm copolymer showed an increased surface roughness for the copolymer (SI-Fig. 2).

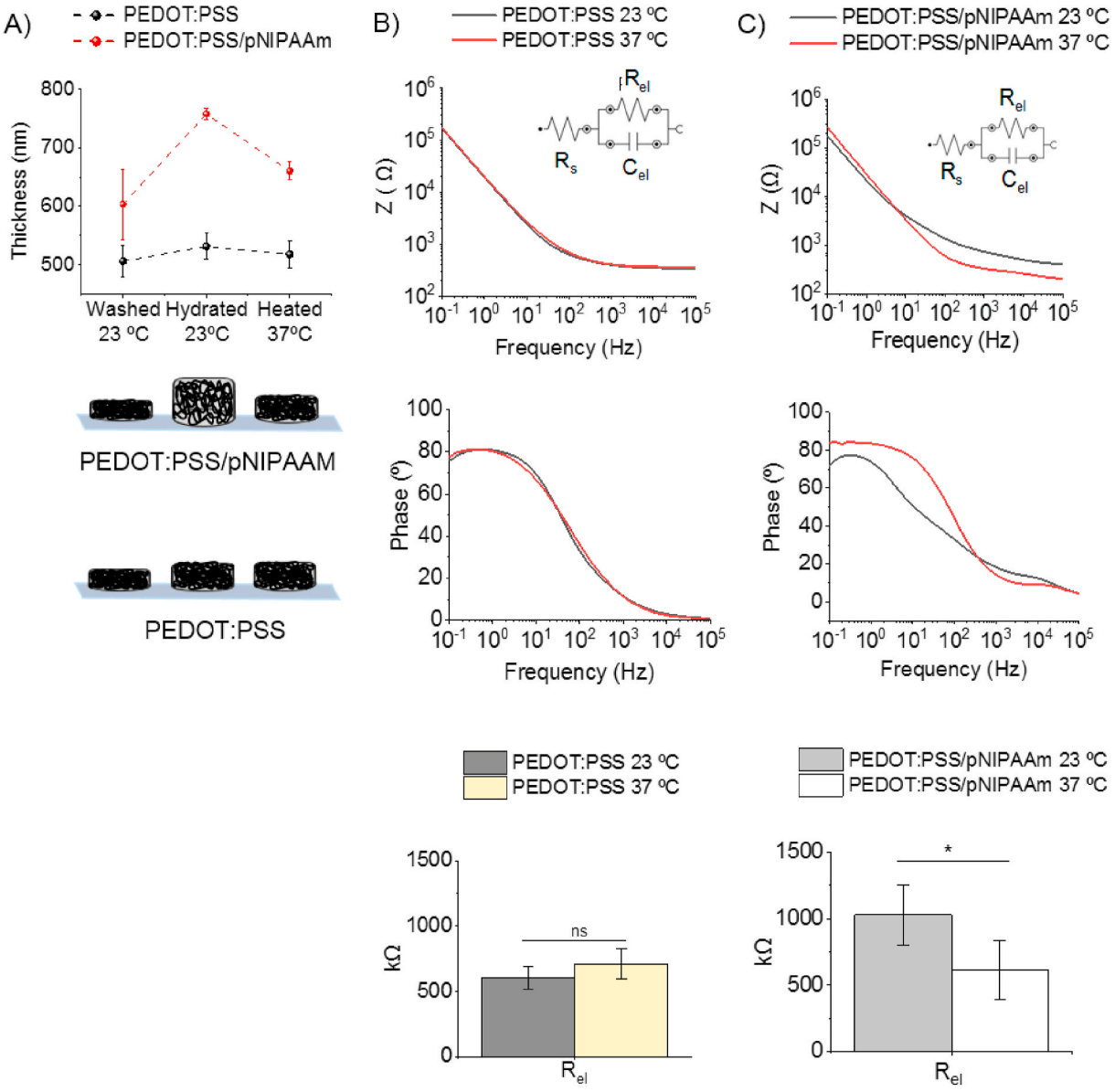


**Fig. 2.** A) Thickness change of PEDOT:PSS and PEDOT:PSS/pNIPAAm after polymerization and during a hydration/heating cycle (top), scheme of the thermo-actuation of PEDOT:PSS/pNIPAAm and PEDOT:PSS (bottom). Error bars correspond to the standard deviation from the mean for n = 4. B) Impedance *vs* frequency (top), phase angle *vs* frequency (middle) and a plot displaying $R_{el}$ (bottom) obtained from EIS measurements of bare the PEDOT:PSS at 23 °C and at 37 °C for a R(RC) circuit. No significantly different (ns) at the 0.05 level (one-way ANOVA $p = 0.2$). Error bars correspond to the standard deviation from the mean for n = 4. C) Impedance *vs* frequency (top), phase angle *vs* frequency (middle) and a plot displaying $R_{el}$ (bottom) obtained from EIS measurements of PEDOT:PSS/pNIPAAm and actuated PEDOT:PSS/pNIPAAm at 37 °C. * Significantly different at the 0.05 level (one-way ANOVA, $p = 0.045$). Error bars correspond to the standard deviation from the mean for n = 4.

We first conducted EIS measurements on all the micro-fabricated electrodes (SI-Figure 3A), as described in detail in section 3 and 4 of the SI. The impedance data showed different impedance profiles for each electrode size (SI-Figure 3B). From this impedance data, the electrode resistance ($R_{el}$) and capacitance ($C_{el}$) were obtained fitting an R(RC) Randles circuit, which evidenced a decreasing resistance and increasing capacitance for bigger electrodes (SI-Figure 3C). Considering the results obtained during characterization, subsequent experiments were carried out with the larger electrodes (rectangular electrodes L = 1.7 mm x W = 1.2 mm) due to the low $R_{el}$ (967 ± 217 kΩ) and high $C_{el}$ (5 ± 2 μF).

To explore the conducting and thermo-responsive properties of the copolymer, the film's thickness at different temperatures was measured with a profilometer. The thickness-change triggered by temperature was investigated for the copolymer and compared to PEDOT:PSS polymer, as it is detailed in the section 5 of SI. The reproducibility of the material (n = 4) was evaluated by assessing the thickness of the swelled and shrunk PEDOT:PSS/pNIPAAm and PEDOT:PSS films was measured just after polymerization, after hydration in DI water for 10 min and after heating the material for 20 min at 37 °C. It is well known that PEDOT:PSS can present high swelling ratios in electrolyte solution (Savva et al., 2018), but this capacity deeply decreases for higher ratios of GOPS (ElMahmoudy et al., 2017). Likewise, low swelling capacity of PEDOT:PSS has previously been reported (Stavrinidou et al., 2013). The PEDOT:PSS films here, with GOPS 3 wt %, showed only a 5% of swelling in cell culture media. The PEDOT:PSS/pNIPAAm copolymer showed a thickness increase of 26% after hydrating, which decreased back to initial values after the thermal treatment. It showed consistent and repetitive changes, demonstrating their predictable thermo-responsive behavior (Fig. 2A). The behavior of the copolymer films correlated well with the previously described performance of pNIPAAm (Tudor et al., 2017). Higher errors were found just after polymerization and washing, due to the differences in hydration of the copolymer after the rinsing of the layers.

PEDOT:PSS/pNIPAAM was also characterized in terms of its electrochemical properties. The volumetric capacitance of the copolymer (section 6 in the SI) was found to be similar to PEDOT:PSS capacitance behavior described by Proctor et al. (2016), showing that the capacitance of PEDOT:PSS/pNIPAAm scales with the volume of the film as a linear function ($y = 2.4x + 3.6 \cdot 10^{-7}$; $R^2 = 0.90$) (SI-Fig. 4). The linearity between capacitance and volume indicates that the ionic charge injected from the electrolyte is uniformly distributed within the dynamic copolymer thus, suggesting that PEDOT:PSS/pNIPAAm films behave as ideal volumetric capacitors. Moreover, we found out that the cpolymer doent lose any conducting or thermos-responsive capability if used within a month demonstrating its long-term stability.

Furthermore, EIS measurements were performed on the materials under study at physiological conditions (in media pH = 7.4), both at swelled and shrunk states at 23 °C and 37 °C, respectively (section 7 in the SI). PEDOT:PSS showed the same impedance profile for both temperatures, and no statistically different $R_{el}$ values (Fig. 2B). In contrast, the impedance profile of PEDOT:PSS/pNIPAAm is significantly different between the swelled state of the copolymer (23 °C) and the shrunk state (37 °C), with a statistically significant value decrease (33%) of $R_{el}$ for the shrunk state (Fig. 2C). This suggests that, although the chemical composition of the copolymer is the same for both states, impedance drops for the shrunk copolymer at the mid-high frequency regime (>10 Hz). In this frequency regime, the electronic transport dominates the impedance spectra of the system. Upon heating, the water is expelled from the polymer film and thus, the polymer film shrinks and the polymer chains become more packed. This might be the reason for the enhanced electronic transport in this material. Furthermore, the impedance of the shrunken PEDOT:PSS/pNIPAAm copolymer at low frequencies (<10 Hz) is larger than PEDOT:PSS, maybe due to the reduced ionic transport properties of the shrunk/contracted polymer film, which hinders ion transport. In addition, the hydrophobic pNIPAAm chains would also hinder the transport of hydrated ions within the polymer film (Zhou et al., 2020). $C_{el}$ did not show any statistical differences for any of the two materials (SI-Fig. 5). PEDOT:PSS, pNIPAAm and PEDOT:PSS/pNIPAAm copolymers were characterized by Raman spectroscopy. The bands corresponding to PEDOT:PSS showed very high intensities, hindering the bands from the pNIPAAm in the copolymer (Section 8 in SI, SI-Fig. 6).

A protocol for the capture and release of cells is included in the supporting information (see section 9 in the SI, SI-Fig. 7). In order to induce cell capture, FN protein, which adheres to the integrins of the cellular membrane, was embedded in the PEDOT:PSS/pNIPAAm electrode to get cell capture functionality. Then, the electrodes were incubated with the cells in media (pH = 7.4) for 3 h and EIS measurements were performed. Different cell densities were tried founding $6.5\ 10^5$ cells $cm^{-2}$ sufficient to undergo the experiments with enough sensitivity. The electrodes with the captured cells were heated to 37 °C for 20 min, above the LCST of pNIPAAm, to trigger the shrinking of the copolymer, and thus the release of the cells due to the conformational changes induced by the thermal actuation of the pNIPAAm (Fig. 1A). EIS measurements evidenced reliable and significantly different changes in impedance measurements with and without captured cells, when using the biggest electrodes (1.7 mm × 1.2 mm rectangle), see section 10 of the SI for electric data and microscopy images of the cell capture and release on the other electrodes, SI-Fig. 8–13, which were not sensitive enough. Fig. 3 shows the results from the cell capture and release experiments on big rectangles, in terms of electrical parameters and optical microscopy.

The impedance data obtained during cell capture and release experiments on PEDOT:PSS/pNIPAAm electrodes display an increased impedance at the mid-high frequencies (>10 Hz) for the samples with cells at 23 °C, with a subsequent recovery of impedance values when temperature-triggered cell release happened (Fig. 3A). The same experiment was conducted with the bare PEDOT:PSS electrodes to demonstrate that the thermo-response of PEDOT:PSS/pNIPAAm triggers cell release (see section 11 in the SI). It was observed that the increase of impedance values detected after cell capture on PEDOT:PSS at 23 °C did not significantly varied when heating the electrodes at 37 °C (SI-Figure 14A). In agreement with the impedance variations, optical microscopy revealed that cells were not released from PEDOT:PSS, as it was confirmed by optical microscopy (SI-Figure 14B). This can be explained due to the absence of pNIPAAm and therefore the possibility of actuating the material.

The experimental data was fitted to a R(RC)(RC) circuit; a R for the electrolyte and two parallel RC circuits, one for the electrode and another for the cell layer on top of the polymer film (Fig. 3B). The corresponding $R_{cells}$ values were calculated for the different stages of the process with PEDOT:PSS and PEDOT:PSS/pNIPAAm electrodes (Fig. 3C). As shown in Fig. 3C, the $R_{cells}$ value of PEDOT:PSS/pNIPAAm was significantly reduced after heating the electrodes (actuation). This reduction of $R_{cells}$, corresponds to a 67% drop value compared to the $R_{cells}$ calculated after cell capture, suggesting that cells were released from the electrode. These results were also supported by optical microscopy (Fig. 3D), where cells detached from the PEDOT:PSS/pNIPAAm surface, and returned to the media (more than 90% of cells detached from all the electrodes). In contrast, the calculated $R_{cells}$ for the PEDOT:PSS with captured cells was not statistically different before and after heating, obtaining values of 687 ± 91 kΩ and 764 ± 135 kΩ, respectively (Fig. 3C). These results suggest that cells remained attached to the copolymer after heating at 37 °C. The results obtained by EIS correlated with the observations by optical microscopy, supporting the use of PEDOT:PSS/pNIPAAm copolymer for cell release upon heating.

In order to confirm the non-invasiveness of the technique, the viability of the released cells was evaluated after every capture and release experiment (see section 12 in the SI). The detached cells were collected in cell culture media and trypan blue was added, which confirmed a cell viability of 94% ± 1 after the cell capture and release process (SI-Figure 15). The results agree with previous studies carried out with bare pNIPAAm, subjected to temperature conformational

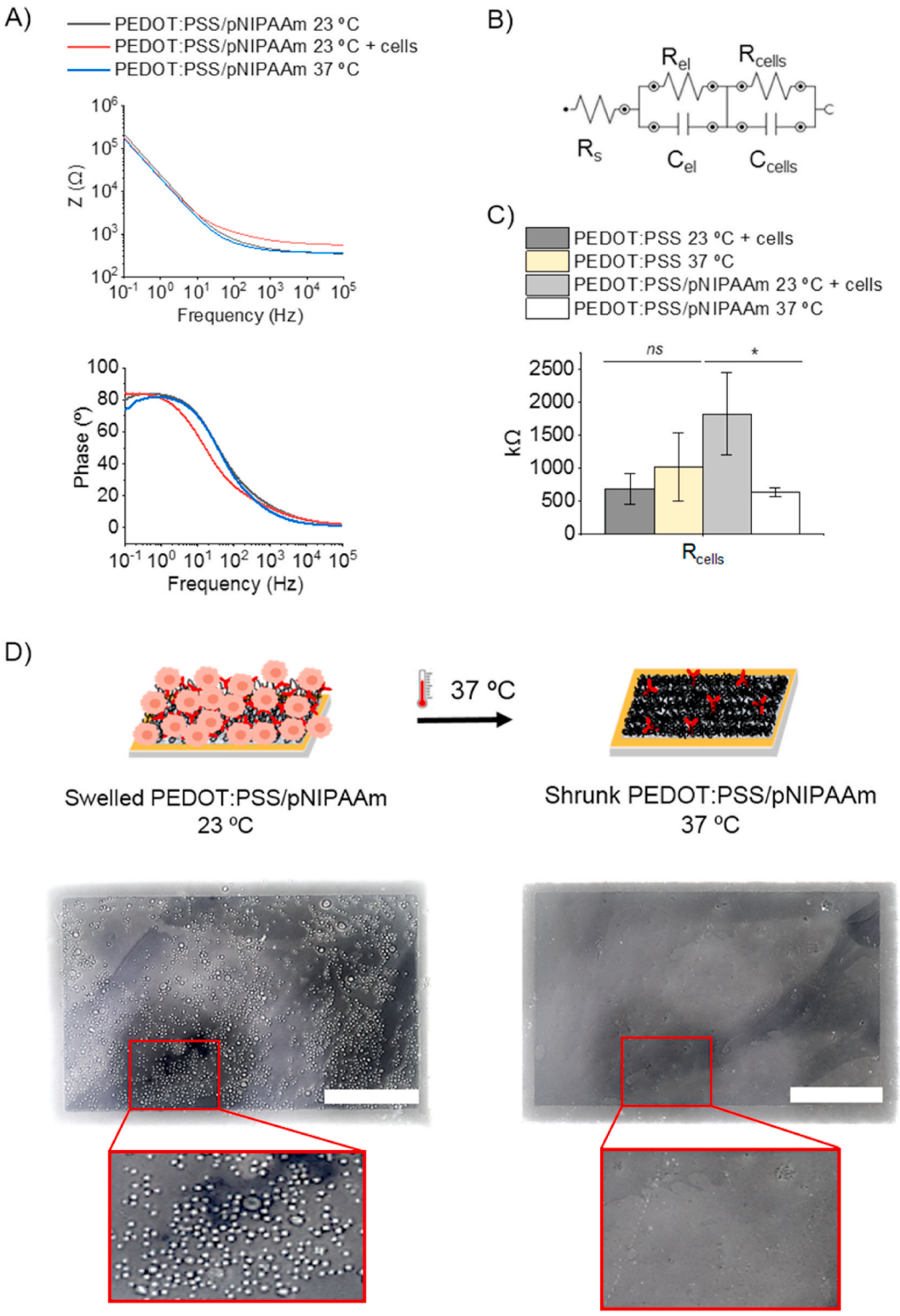


**Fig. 3.** Cell capture and release data. A) Impedance *vs* frequency and phase *vs* frequency plots of the cell capture and release with PEDOT:PSS/pNIPAAm. B) R(RC)(RC) electric circuit fitting for this system. C) $R_{cells}$ plotted for PEDOT:PSS and PEDOT:PSS/pNIPAAm with cells at 23 °C and at 37 °C after heating. Error bars correspond to the standard deviation from the mean for four different samples n = 4. *N*ot significantly different *(ns)* at the 0.05 level (one-way ANOVA $p = 0.29$) and * significantly different at the 0.05 level (one-way ANOVA, $p = 0.009$). D) Scheme of the actuation process and optical microscopy images of the captured cells (left) and after thermo-actuation (right) (4x) with a zoomed fraction of 400 × 200 μm area. Scale bars correspond to 400 μm.

changes (Wang et al., 2016; Liu et al., 2013a,b; Gurkan et al., 2011).

The presence of the protein in the copolymer, during cell capture and release, was investigated. Bovine serum albumin (BSA) model protein (Swain and Sarkar, 2013; Naddaf et al., 2010) was used to study the stability of adhesion proteins in the copolymer by fluorescence intensity measurements of the polymer surface. The polymeric films: PEDOT:PSS, pNIPAAm and PEDOT:PSS/pNIPAAm were soaked in the fluorescent labelled tetramethylrhodamine conjugated albumin from bovine serum

(BSA-TAMRA). The presence of the protein on the films was monitored during the process of capture and release (see section 13 in the SI). The polymeric layers were fabricated as described in the section 2 of the SI, and incubated with 500 nM of BSA-TAMRA for 2 h. The protein was tracked by fluorescence microscopy at room temperature, after incubation, and after heating the samples for 20 min at 37 °C. The protein adsorbed more in the copolymer containing the pNIPAAm than in PEDOT:PSS, which may explain the lower cell adhesion observed for the PEDOT:PSS electrodes. The pNIPAAm hydrogel integrated the protein more efficiently but after actuation only 38% of the adsorbed protein remained in the polymer, while in the PEDOT:PSS/pNIPAAm copolymer 51% was retained (SI-Figure 16). A similar percentage, 44% of the protein release, was observed by UV–Vis spectrometry for the FN after polymer actuation (see section 13 in the SI, SI-Figure 17). That can be explained because the presence of PEDOT:PSS diminishes the shrinking of the pNIPAAm, reducing the protein release. Although 51% of protein remained in the copolymer after actuation, according to fluorescence microscopy, all the cells were released, suggesting that the conformational change triggers cell release, regardless of the percentage of protein remaining in the copolymer. In addition, the density of captured cells per area on the electrodes was estimated by dividing the microscopy images of captured cells of each big square electrode in 3 sub-squares of 500 × 500 μm, and the cells of this area were counted. The density of captured cells was 483 ± 61 cells per 500 × 500 μm area for PEDOT:PSS/pNIPAAm, and 175 ± 98 cells per 500 × 500 μm square for PEDOT:PSS (Fig. 3D and SI-Figure 14B) (n = 3 different electrodes). That is explained considering the higher water uptake of the copolymer due to the pNIPAAm, which helps accommodating large amounts of FN solution, increasing the presence of protein within the copolymer (SI-Figure 16) and thus, creating more adhesion sites for cells. Moreover, PEDOT:PSS showed high variability in the density of captured cells for both, within the same electrode and between electrodes, while the cell coverage on PEDOT:PSS/pNIPAAm was more homogeneous for these two comparisons.

In conclusion, the functional material PEDOT:PSS/pNIPAAm copolymer was deposited on gold electrodes and functionalized with FN to promote the capture of cancer cells. The novel copolymer maintained similar electrical properties to the ones of PEDOT:PSS, enabling the system to be sensitive enough to detect the target, while maintaining the thermo-actuation capability of the pNIPAAm. Therefore, PEDOT:PSS/pNIPAAm copolymer is functional for temperature triggered release of hosting cells, as well as for the simultaneous monitoring of the process by EIS. This opens the possibility of using organic bioelectronics as sensors and actuators, as label-free devices to perform the detection and recovery of target species, leading to an easy track of the process without labels, and minimum user intervention. These results present the first step on the development of more complex architectures that can act simultaneously as a sensor and actuator of different targets, while monitoring its performance electrically. Therefore, there is a great potential to adapt this platform, by changing the capturing specific molecule, to be used for the collection of other cells such as blood cells, CTCs, bacteria or even exosomes with relatively high temporal resolution. This type of measurement will open the floodgates to the fast diagnostic of cancer at the point-of-care in clinic.

## Experimental section

A detailed description of procedures and characterization methods are available in the Supporting Information.

## CRediT authorship contribution statement

**Maite Garcia-Hernando:** Conceptualization, Methodology, Investigation, Formal analysis, Writing – original draft, Writing – review & editing, Funding acquisition. **Janire Saez:** Conceptualization, Supervision, Methodology, Investigation, Writing – original draft, Writing – review & editing, Funding acquisition. **Achilleas Savva:** Formal analysis, Writing – original draft, Writing – review & editing. **Lourdes Basabe-Desmonts:** Conceptualization, Writing – review & editing, Funding acquisition. **Róisín M. Owens:** Writing – review & editing, Funding acquisition. **Fernando Benito-Lopez:** Conceptualization, Supervision, Writing – review & editing, Funding acquisition.

## Declaration of competing interest

The authors declare that they have no known competing financial interests or personal relationships that could have appeared to influence the work reported in this paper.

## Acknowledgments

This project has received funding from University of the Basque Country (PIF16/204 and MOV19/41), the European Union's Horizon 2020 research and innovation programme under the Marie Skłodowska-Curie grant agreement No. 842356, Gobierno de España, Ministerio de Economía y Competitividad, with Grant No. BIO2016-80417-P (AEI/FEDER, UE) and Gobierno Vasco Dpto. Educación for the consolidation of the research groups (IT1271-19).

## Appendix A. Supplementary data

Supplementary data to this article can be found online at https://doi.org/10.1016/j.bios.2021.113405.

## References

Bartolome, R., Barderas, R., Torres, S., Fernandez-Aceñero, M.J., Mendes, M., García-Foncillas, J., Lopez-Lucendo, M., Casal, J.I., 2014. Oncogene 33, 1658–1669.
Bhagwat, N., Dulmage, K., Pletcher, C.H., Wang, L., DeMuth, W., Sen, M., Balli, D., Yee, S.S., Sa, S., Tong, F., 2018. Sci. Rep. 8, 1–14.
Bird, C., Kirstein, S., 2009. Nat. Methods 6, v–vi.
Bombera, R., Leroy, L., Livache, T., Roupioz, Y., 2012. Biosens. Bioelectron. 33, 10–16.
Cantor, D.I., Cheruku, H.R., Nice, E.C., Baker, M.S., 2015. Canc. Metastasis Rev. 34, 715–734.
Cao, J., Zhao, X., Younis, M.R., Li, Z., Xia, X., Wang, C., 2017. Anal. Chem. 89, 10957–10964.
Chawla, K., Bürgel, S.C., Schmidt, G.W., Kaltenbach, H., Rudolf, F., Frey, O., Hierlemann, A., 2018. Microsyst Nanoeng 4, 1–12.
Choi, A., Seo, K.D., Yoon, H., Han, S.J., Kim, D.S., 2019. Biomater. Sci. 7, 2277–2287.
Cui, H., Liu, Q., Li, R., Wei, X., Sun, Y., Wang, Z., Zhang, L., Zhao, X., Hua, B., Guo, S., 2020. Nanoscale 12, 1455–1463.
Curto, V., Ferro, M., Mariani, F., Scavetta, E., Owens, R., 2018. Lab Chip 18, 933–943.
Del Agua, I., Marina, S., Pitsalidis, C., Mantione, D., Ferro, M., Iandolo, D., Sanchez-Sanchez, A., Malliaras, G.G., Owens, R.M., Mecerreyes, D., 2018. ACS Omega 3, 7424–7431.
ElMahmoudy, M., Inal, S., Charrier, A., Uguz, I., Malliaras, G.G., Sanaur, S., 2017. Macromol. Mater. Eng. 302, 1600497.
Fan, Z., Ouyang, J., 2019. Adv. Electron. Mater. 5, 1800769.
Fathi, F., Rahbarghazi, R., Rashidi, M., 2018. Biosens. Bioelectron. 101, 188–198.
Gallagher, S., Kavanagh, A., Zíołkowski, B., Florea, L., MacFarlane, D.R., Fraser, K., Diamond, D., 2014. Phys. Chem. Chem. Phys. 16, 3610–3616.
Gao, T., Li, L., Wang, B., Zhi, J., Xiang, Y., Li, G., 2016. Anal. Chem. 88, 9996–10001.
Gaysinskaya, V., Soh, I.Y., van der Heijden, Godfried, W., Bortvin, A., 2014. Cytometry Part A 85, 556–565.
Gupta, S.K., Oommen, S., Aubry, M., Williams, B.P., Vlahakis, N.E., 2013. Oncogene 32, 141–150.
Gurkan, U.A., Anand, T., Tas, H., Elkan, D., Akay, A., Keles, H.O., Demirci, U., 2011. Lab Chip 11, 3979–3989.
Hao, Y., Liu, H., Li, G., Cui, H., Jiang, L., Wang, S., 2018. ChemPhysChem 19, 2107–2112.
Hartman, J., Edvardsson, K., Lindberg, K., Zhao, C., Williams, C., Strom, A., Gustafsson, J.A., 2009. Canc. Res. 69, 6100–6106.
Henry, E., Holm, S.H., Zhang, Z., Beech, J.P., Tegenfeldt, J.O., Fedosov, D.A., Gompper, G., 2016. Sci. Rep. 6, 34375.
Hisey, C.L., Dorayappan, K.D.P., Cohn, D.E., Selvendiran, K., Hansford, D.J., 2018. Lab Chip 18, 3144–3153.
Hou, S., Zhao, H., Zhao, L., Shen, Q., Wei, K.S., Suh, D.Y., Nakao, A., Garcia, M.A., Song, M., Lee, T., 2013. Adv. Mater. 25, 1547–1551.
Iandolo, D., Sheard, J., Levy, G.K., Pitsalidis, C., Tan, E., Dennis, A., Kim, J., Markaki, A. E., Widera, D., Owens, R.M., 2020. MRS Commun 10, 179–187.
Jimison, L.H., Tria, S.A., Khodagholy, D., Gurfinkel, M., Lanzarini, E., Hama, A., Malliaras, G.G., Owens, R.M., 2012. Adv. Mater. 24, 5919–5923.

Johnson, S.P., Catania, J.M., Harman, R.J., Jensen, E.D., 2012. Stem Cell. Dev. 21, 2949–2957.
Kang, Y., Kim, Y.J., Bu, J., Cho, Y., Han, S., Moon, B., 2017. Nanoscale 9, 13495–13505.
Ke, N., Wang, X., Xu, X., Abassi, Y.A., 2011. The xCELLigence system for real-time and label-free monitoring of cell viability. In: Mammalian Cell Viability. Springer, pp. 33–43.
Kumar, P., Vriens, K., Cornaglia, M., Gijs, M., Kokalj, T., Thevissen, K., Geeraerd, A., Cammue, B., Puers, R., Lammertyn, J., 2015. Lab Chip 15, 1852–1860.
Legut, M., Sanjana, N.E., 2019. Nat. Biomed. Eng. 3, 759–760.
Leibovitz, A., Stinson, J.C., McCombs, W.B., McCoy, C.E., Mazur, K.C., Mabry, N.D., 1976. Canc. Res. 36, 4562–4569.
Li, J., Qi, C., Lian, Z., Han, Q., Wang, X., Cai, S., Yang, R., Wang, C., 2016. ACS Appl. Mater. Interfaces 8, 2511–2516.
Liu, H., Liu, X., Meng, J., Zhang, P., Yang, G., Su, B., Sun, K., Chen, L., Han, D., Wang, S., 2013a. Adv. Mater. 25, 922–927.
Liu, S., Chen, X., Bao, L., Liu, T., Yuan, P., Yang, X., Qiu, X., Gooding, J.J., Bai, Y., Xiao, J., 2020. Nat. Biomed. Eng. 4, 1063–1075.
Liu, S., Wang, J., Niu, W., Liu, E., Wang, J., Peng, C., Lin, P., Wang, B., Khan, A.Q., Gao, H., 2013b. Canc. Lett. 328, 325–334.
Lu, Y., Ahmed, S., Harari, F., Vahter, M., 2015. J. Trace Elem. Med. Biol. 29, 249–254.
Malic, L., Zhang, X., Brassard, D., Clime, L., Daoud, J., Luebbert, C., Barrere, V., Boutin, A., Bidawid, S., Farber, J., 2015. Lab Chip 15, 3994–4007.
Naddaf, A., Tsibranska, I., Bart, H., 2010. Chem. Eng. Process 49, 581–588.
Proctor, C.M., Rivnay, J., Malliaras, G.G., 2016. J. Polym. Sci., Part B: Polym. Phys. 54, 1433–1436.
Qian, W., Zhang, Y., Chen, W., 2015. Small 11, 3850–3872.
Rabie, H., Zhang, Y., Pasquale, N., Lagos, M.J., Batson, P.E., Lee, K., 2019. Adv. Mater. 31, 1806991.
Reitinger, S., Wissenwasser, J., Kapferer, W., Heer, R., Lepperdinger, G., 2012. Biosens. Bioelectron. 34, 63–69.
Rivnay, J., Ramuz, M., Leleux, P., Hama, A., Huerta, M., Owens, R.M., 2015. Appl. Phys. Lett. 106, 8_1.
Ruan, H., Wu, X., Yang, C., Li, Z., Xia, Y., Xue, T., Shen, Z., Wu, A., 2018. ACS Biomater. Sci. Eng. 4, 1073–1082.
Savva, A., Wustoni, S., Inal, S., 2018. J. Mater. Chem. 6, 12023–12030.
Shen, H., Ma, J.L., Zhang, Y., Deng, G.L., Qu, Y.L., Wu, X.L., He, J.X., Zhang, S., Zeng, S., 2016. World J. Gastroenterol. 22, 3969–3977.
Shen, Q., Xu, L., Zhao, L., Wu, D., Fan, Y., Zhou, Y., OuYang, W., Xu, X., Zhang, Z., Song, M., 2013. Adv. Mater. 25, 2368–2373.
Song, Y., Shi, Y., Huang, M., Wang, W., Wang, Y., Cheng, J., Lei, Z., Zhu, Z., Yang, C., 2019. Angew. Chem. Int. Ed. 58, 2236–2240.
Stavrinidou, E., Leleux, P., Rajaona, H., Khodagholy, D., Rivnay, J., Lindau, M., Sanaur, S., Malliaras, G.G., 2013. Adv. Mater. 25, 4488–4493.
Steinem, C., Janshoff, A., Galla, H., Sieber, M., 1997. Bioelectrochem. Bioenerg. 42, 213–220.
Stolwijk, J.A., Wegener, J., 2019. Label-Free Monitoring of Cells in Vitro, pp. 1–75.
Swain, S.K., Sarkar, D., 2013. Appl. Surf. Sci. 286, 99–103.
Tudor, A., Saez, J., Florea, L., Benito-Lopez, F., Diamond, D., 2017. Sensor. Actuator. B Chem. 247, 749–755.
Umapathi, R., Reddy, P.M., Kumar, A., Venkatesu, P., Chang, C., 2015. Colloids Surf., B 135, 588–595.
Wang, L., Liu, H., Zhang, F., Li, G., Wang, S., 2016. Small 12, 4697–4701.
Wang, W., Chen, P., Hsiao, H., Wang, H., Liang, W., Su, Y., 2004. Oncogene 23, 6666–6671.
Xia, Y., Ouyang, J., 2012. ACS Appl. Mater. Interfaces 4, 4131–4140.
Xia, Y., Tang, Y., Yu, X., Wan, Y., Chen, Y., Lu, H., Zheng, S., 2017. Small 13, 1603135.
Yamada, M., Seko, W., Yanai, T., Ninomiya, K., Seki, M., 2017. Lab Chip 17, 304–314.
Zhan, W., Wei, T., Cao, L., Hu, C., Qu, Y., Yu, Q., Chen, H., 2017. ACS Appl. Mater. Interfaces 9, 3505–3513.
Zhao, W., Cui, C.H., Bose, S., Guo, D., Shen, C., Wong, W.P., Halvorsen, K., Farokhzad, O. C., Teo, G.S., Phillips, J.A., Dorfman, D.M., Karnik, R., Karp, J.M., 2012. Proc. Natl. Acad. Sci. U.S.A. 109, 19626–19631.
Zhou, Q., Teng, W., Jin, Y., Sun, L., Hu, P., Li, H., Wang, L., Wang, J., 2020. Electrochim. Acta 334, 135530.